J. Fluid Mech. (2023), *vol*. 956, R2, doi:10.1017/jfm.2023.9

Freeze-out of perturbation growth of single-mode helium–air interface through reflected shock in Richtmyer–Meshkov flows

Chenren Chen[1], **Yinuo Xing**[1], **He Wang**[1], **Zhigang Zhai**[1,†] **and Xisheng Luo**[1]

[1] Advanced Propulsion Laboratory, Department of Modern Mechanics, University of Science and Technology of China, Hefei 230026, PR China

(Received 21 September 2022; revised 24 November 2022; accepted 2 January 2023)

'Freeze-out' of amplitude growth, i.e. the amplitude growth stagnation of a shocked helium–air interface, is realized through a reflected shock, which produces baroclinic vorticity of the opposite sign to that deposited by the first shock. Theoretically, a model is constructed to calculate the relations among the initial parameters for achieving freeze-out. In particular, if the amplitude growth is within the linear regime at the arrival of the reflected shock, the time interval between the impacts of two shock waves is linearly related to the initial perturbation wavelength, and is independent of the initial perturbation amplitude. Experimentally, an air–SF_6 (or air–argon) plane interface is adopted to produce a weak reflected shock. Seven experimental runs with specific initial conditions are examined. For all cases, freeze-out is achieved after the reflected shock impact under the designed conditions.

Key words: shock waves

1. Introduction

When a shock wave passes through a perturbed interface separating two fluids with different densities, the Richtmyer–Meshkov (RM) (Richtmyer 1960; Meshkov 1969) instability occurs. The development of the RM instability is mainly driven by baroclinic vorticity produced by misalignment of the pressure and density gradients. It is hoped to be able to manipulate the RM instability, because it is a significant obstacle to the realization of inertial confinement fusion (ICF) (Lindl *et al.* 2014). For a single-shocked interface, the perturbation amplitude will experience a linear growth, then continue to grow nonlinearly, and finally may reach a turbulent mixing stage. If the single-shocked interface experiences a second shock impact, additional vorticity will be produced. This provides a possibility to manipulate the amplitude growth rate through multiple shock impacts.

† Email address for correspondence: sanjing@ustc.edu.cn

The idea that the RM instability can be manipulated through a second shock impact was first theoretically proposed by Mikaelian (1985). If the amplitude growth rate induced by the second shock exactly cancels the growth rate caused by the first shock, the amplitude growth will stagnate, which is called 'freeze-out'. To achieve freeze-out, the second shock should produce baroclinic vorticity of the opposite sign to that deposited by the first shock. For a heavy–light interface after the phase inversion, the second shock must propagate in the same direction as the first shock; whereas for a light–heavy interface, the second shock should propagate in the opposite direction to the first shock. By superimposing the impulsive model (Richtmyer 1960), Mikaelian (1985) constructed a simple model to predict the time interval between the impacts of two shock waves to achieve freeze-out.

In numerical simulations, freeze-out of a heavy–light interface perturbation was realized through the impacts by two successive shock waves, i.e. two shock waves travelling in the same direction (Charakhch'yan 2000, 2001). More recently, freeze-out of a light–heavy interface perturbation was realized through a weaker reflected shock (Mikaelian 2010).

In experiments, two successive shock waves are difficult to generate in an ordinary shock tube and, therefore, experimental studies on freeze-out of a heavy–light interface perturbation are rare. A reflected shock has generally been produced through an incident shock reflecting from a rigid wall (Weber *et al.* 2012; Jacobs *et al.* 2013; Mohaghar *et al.* 2019; Guo *et al.* 2022). Such a reflected shock, however, is often too strong to realize freeze-out of a light–heavy perturbation. To reduce the reflected shock intensity, elastomeric foam was adopted as a 'soft wall' by Leinov *et al.* (2009) to study the development of a light–heavy interface. Up to now, however, the experimental work on freeze-out of a light–heavy perturbation is scarce, which motivates the current work.

In this work, freeze-out of a single-mode helium–air interface accelerated by an incident shock and its reflected shock is investigated. We shall first construct a model to determine the freeze-out condition when the perturbation growth of the first-shocked interface is within the linear or weakly nonlinear stage at the arrival of the reflected shock. At the linear stage, the perturbation amplitude grows linearly, and crests and troughs of the interface develop symmetrically. At the weakly nonlinear stage, the amplitude begins to grow nonlinearly and asymmetric structures (bubble and spike) appear. However, the interface is still smooth and simply connected, and small vortices have not arisen on the spike's shoulder (Liu *et al.* 2018; Zhou *et al.* 2021). To produce a weak reflected shock, a planar gas interface, instead of a rigid wall, is adopted. Then, the corresponding experiments are designed and conducted by using the initial configurations obtained from the model. It will be shown that, for both the linear and weakly nonlinear cases, freeze-out can be achieved after the reflected shock impact under the designed conditions.

2. Theoretical analysis

There are two assumptions for the theoretical analysis. First, the post-shock interface satisfies the small-perturbation hypothesis, namely, $a_1^-/\lambda < 0.1$, with λ and a_1^- being the wavelength and amplitude of the perturbation, when the reflected shock arrives. Second, the amplitude growth rates induced by the incident shock and the reflected shock follow the linear superposition principle (Mikaelian 1985), i.e. $v = v_i + v_r$, where v is the amplitude growth rate after the reflected shock impact, v_i is the growth rate induced by the incident shock just before the reflected shock impact and v_r is the linear growth rate induced by the reflected shock. Note that v_i here is not limited to the linear growth rate induced by the incident shock.

For the development of a single-mode light–heavy interface perturbation induced by a planar shock wave, the nonlinear model proposed by Zhang & Guo (2016) (the ZG model) is adopted, since it has been widely verified to predict v_i in linear and weakly nonlinear regimes (Liu *et al.* 2018; Liang *et al.* 2019; Guo *et al.* 2022). The ZG model can be expressed as

$$v_i = v_i^{ZG}(t) = \frac{1}{2}[v_b^{ZG}(t) + v_s^{ZG}(t)], \quad v_{b/s}^{ZG}(t) = \frac{v_i^R}{1 + \theta k v_i^R t}, \tag{2.1a,b}$$

where $v_{b/s}$ is the amplitude growth rate of the bubble or spike, v_i^R is the linear growth rate calculated by the impulsive model (Richtmyer 1960) and

$$\theta = \frac{3}{4}\frac{(1+A^+)(3+A^+)}{[3+A^+ + \sqrt{2}(1+A^+)^{1/2}]}\frac{[4(3+A^+) + \sqrt{2}(9+A^+)(1+A^+)^{1/2}]}{[(3+A^+)^2 + 2\sqrt{2}(3-A^+)(1+A^+)^{1/2}]}. \tag{2.2}$$

Here, A^+ is the post-shock Atwood number, defined as $A^+ = (\rho_2^+ - \rho_1^+)/(\rho_2^+ + \rho_1^+)$ with ρ_1^+ and ρ_2^+ being the densities of the light and heavy fluids on both sides of the perturbed interface, after the incident shock impact. In the above, v_i^R can be described as

$$v_i^R = C_1 k a_0 A^+ \Delta u, \tag{2.3}$$

where a_0 is the initial perturbation amplitude, C_1 is the incident shock compression factor (Meshkov 1969) and Δu is the interface velocity jump induced by the incident shock.

Through the ZG model, the perturbation amplitude just before the reflected shock impact, $a_1^- = a_0 C_1 + \int_0^{\Delta t} v_i^{ZG}(t)\,\mathrm{d}t$, can be provided, in which Δt is the time interval between the impacts of two shock waves. Specifically, if the amplitude growth is within the linear stage when the reflected shock arrives, v_i can be directly predicted by the impulsive model, i.e. $v_i = v_i^R$. In this work, to ensure the validity of the ZG model, only the linear and weakly nonlinear stages of the amplitude growth are involved.

When the reflected shock impacts the evolving heavy–light interface, rarefaction waves are reflected. The irrotational model proposed by Wouchuk & Nishihara (1997) (the WN model) has been verified to accurately predict the linear growth rate of a shocked single-mode interface when a rarefaction wave is reflected (Wouchuk 2001). In the present work, the linear growth rate induced by the reflected shock v_r can be predicted by the WN model as

$$v_r = k a_1^- f(M_{s1}, M_{s2}, \rho_1, \rho_2, \gamma_1, \gamma_2). \tag{2.4}$$

Here, ρ_1 and ρ_2 (γ_1 and γ_2) are the initial densities (specific heat ratios) of the light and heavy fluids on both sides of the perturbed interface, while M_{s1} and M_{s2} are the Mach numbers of the incident shock and reflected shock when they encounter the interface. The function f can be expressed as

$$f = \frac{\rho_{1r}\Delta u_r\left(1 - \dfrac{V_{rt}}{V_{rs}}\right) + \rho_{2r}(\Delta u_{2r} - \Delta u_r)\left(1 + \dfrac{V_{rf}}{V_{rs}}\right)}{\rho_{1r} + \rho_{2r}}. \tag{2.5}$$

Here, ρ_{1r} and ρ_{2r} are the densities of the light and heavy fluids on both sides of the interface after the reflected shock impact; V_{rs}, V_{rf} and V_{rt} are the velocities of the reflected shock, the rarefaction wave front and the re-transmitted shock, respectively; and Δu_r and Δu_{2r} are the interface velocity jumps induced by the reflected shock and the heavy fluid

Case	L_0	a_0	λ	a_0/λ	a_1^-/λ	M_{s1}	M_{s2}	φ(He)	A^+	Δt	Δu^e	Δu^t	Δu_r^e	Δu_r^t
1	105	0.94	60	0.016	0.040	1.19	1.05	0.70	0.44	420	123.3	125.9	37.3	38.6
2	70	0.60	40	0.015	0.040	1.19	1.05	0.70	0.44	290	125.2	127.8	37.9	38.6
3	80	0.60	40	0.015	0.037	1.20	1.05	0.65	0.40	340	129.3	127.3	38.2	37.5
4	60	0.44	30	0.015	0.033	1.19	1.05	0.64	0.39	260	120.7	119.6	38.6	37.1
5	110	0.26	20	0.013	0.064	1.20	1.02	0.68	0.44	440	129.8	127.8	15.5	15.6
6	80	0.53	20	0.026	0.110	1.19	1.02	0.71	0.45	350	122.6	123.4	14.5	15.7
7	60	0.80	20	0.040	0.138	1.18	1.02	0.73	0.46	300	121.5	122.5	19.1	21.4

Table 1. Parameters in all cases: L_0 is the distance from the average position of the single-mode helium–air interface to the planar air–SF_6 (air–argon) interface; a_0 is the initial amplitude and a_1^- is the amplitude just before the reflected shock arrival; λ is the perturbation wavelength; M_{s1} and M_{s2} are the Mach numbers of the incident shock and reflected shock; φ(He) is the helium volume fraction in space A; A^+ is the post-shock Atwood number; Δt is the time interval between the impacts of two shock waves; and Δu and Δu_r are the helium–air interface velocity jumps induced by the incident shock and reflected shock. The superscripts 't' and 'e' denote theoretical and experimental results. The units for length, velocity and time are mm, m s^{-1} and μs, respectively.

velocity after the reflected shock impact. These parameters in (2.5) can be solved using one-dimensional (1-D) gas dynamics theory by providing shock Mach numbers and initial parameters.

According to the analysis above, v can be theoretically predicted if the initial parameters are provided. When $v = 0$, the interface amplitude remains constant after the reflected shock impact, i.e. the amplitude growth is 'frozen out'. The relationship among the initial parameters can be determined to realize freeze-out by using (2.1*a*,*b*) to (2.5). In particular, if v_i belongs to the linear growth rate regime, the freeze-out condition is independent of a_0. When the shock intensities and the properties of the gases on both sides of the interface are fixed, to realize freeze-out, the initial perturbation wavelength (λ) and Δt satisfy a linear relationship:

$$\Delta t/\lambda = -(f + A^+\Delta u)/(2\pi f A^+\Delta u). \tag{2.6}$$

This relationship in the $(\lambda, \Delta t)$ plane is called the freeze-out line. However, if the amplitude grows nonlinearly at the arrival of the reflected shock, the freeze-out condition is also dependent upon a_0, and such a linear relationship between λ and Δt does not exist.

3. Experimental method

Experiments are performed to achieve freeze-out under the proper conditions determined by the model. To produce a weak reflected shock, a planar air–SF_6 (sulfur hexafluoride) or air–argon interface, instead of a rigid wall, is adopted. Selection of either SF_6 or argon is dependent on the reflected shock strength. If the amplitude growth is linear (weakly nonlinear) when the reflected shock arrives, an air–SF_6 (air–argon) interface is adopted to generate a relatively strong (weak) reflected shock. The intensities of the reflected shock waves when using these different gas combinations are listed in table 1.

The soap film technique (Liu *et al.* 2018; Liang *et al.* 2019) is adopted to create the interfaces. As shown in figures 1(*a*) and 1(*b*), there are three interfaces, including a perturbed one and two undisturbed ones. The first interface AI_1 (undisturbed) is used to separate helium (in space A) from air in the driven section; the second interface II (perturbed) to separate air (in space B) from helium (in space A) to create a single-mode helium–air interface; and the third interface AI_2 (undisturbed) to separate SF_6 or argon (in

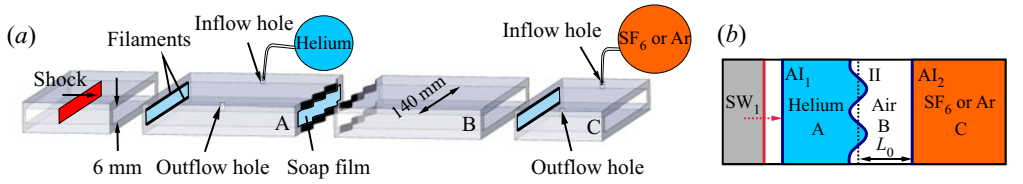

Figure 1. Schematics of the soap film interface generation (*a*) and the initial configuration studied (*b*). Here, AI_1 and AI_2 are two undisturbed auxiliary interfaces; II is the initial helium–air interface; SW_1 is the incident shock; and L_0 is the initial distance between II and AI_2.

space C) from air (in space B) for reflecting a weak shock. To generate the interfaces separating the different gases, after the soap film interfaces are formed at the preset positions, light gas (helium) and heavy gas (SF_6 or argon) are pumped into spaces A and C, respectively, through the inflow holes, and air is slowly discharged through the outflow holes.

For all experimental runs, the inflation rate and duration are the same to ensure similar volume fractions of light and heavy gases in the spaces as far as possible. Because helium is easily polluted, the contamination of helium by air in space A is considered, whereas the gases in the other spaces are considered as pure. The helium concentration is determined by comparing the measured velocities of the incident shock, the transmitted shock and the helium–air interface velocity jump in experiments with those predicted from 1-D gas dynamics theory. The distance between II and AI_1 is 100 mm, which is large enough to ensure that the interface-coupling effect and the disturbance waves will not affect the development of the helium–air perturbation (Liang & Luo 2021). The distance between II and AI_2 is defined as L_0, which is flexible to change the time interval Δt.

The experiments are conducted in a horizontal shock tube (Guo *et al.* 2022), and the Mach number of the incident plane shock moving in helium is 1.19 ± 0.01. The post-shock flow field is recorded by high-speed schlieren photography. The frame rate of the camera (FASTCAM SA5, Photron Ltd) is 50 000 frames per second and the exposure time is 1 μs. Owing to the different sizes of the observation domains required, the spatial resolution ranges from 0.38 to 0.45 mm pixel^{-1}. The ambient pressure and temperature are 101.3 ± 0.1 kPa and 295 ± 1.5 K, respectively. We note that, due to the limitation of the observation window, the developments of these three interfaces cannot be captured simultaneously by the camera. Since the emphasis is on the development of the single-mode interface, in the following experiments, both helium–air and air–SF_6 (or air–argon) interfaces (II and AI_2) are shown in the schlieren images, whereas the air–helium interface (AI_1) is absent.

4. Results and discussion

4.1. *Unperturbed case*

In experiments, we first verify that AI_1 will not affect the development of II. For this purpose, the movements of AI_1 and the undisturbed II after shock impact are studied, and the corresponding schlieren images are presented in figure 2(*a*). The initial time is defined as the moment when the incident shock (SW_1) meets the interface, and similarly hereinafter. As SW_1 impinges on II, a transmitted shock wave (SW_1^t) and a once-shocked helium–air interface (OSI) are formed. During the time studied, the shocked AI_1 (SAI) is always far away from the OSI. Note that SAI is deformed slightly after it passes across the

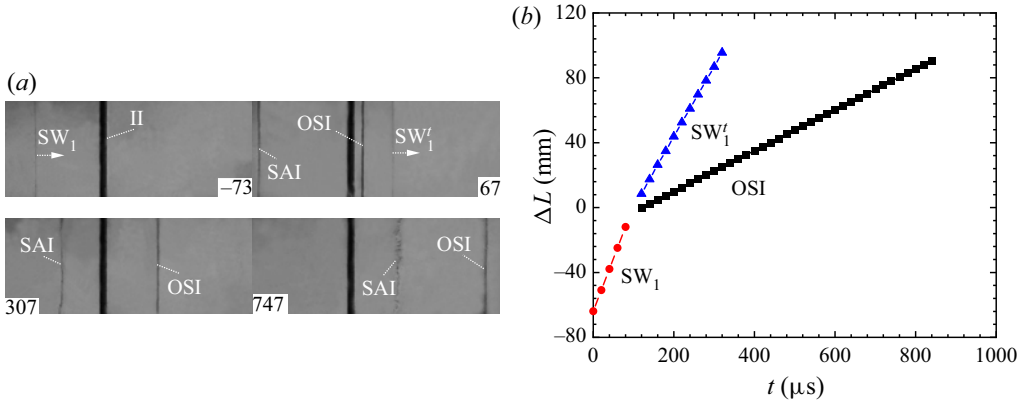

Figure 2. Evolution of a plane helium–air interface induced by a plane shock (*a*) and the trajectories of the interface and the shock waves (*b*). Here, ΔL is the distance of the evolving interface from the initial position of II; OSI is the once-shocked interface; SAI is the shocked auxiliary interface; and SW_1^t is the first transmitted shock. Other symbols have the same meaning as those in figure 1.

holes (307 μs). Later, the small disturbances on SAI develop significantly (747 μs), which is primarily caused by the filaments used to restrict the soap film interface. However, the disturbances on the OSI can still be ignored, which is consistent with the previous work in helium layers (Liang & Luo 2021). Therefore, the interface-coupling effect is negligible.

The trajectories of the shock waves and OSI extracted from the schlieren images are shown in figure 2(*b*). Both the shock waves and OSI move linearly, which means that the OSI has not been affected significantly by additional waves except SW_1. Through measuring the velocities of the shock waves and OSI, and combining with 1-D gas dynamics theory, the volume fraction of helium in space A is calculated to be $68\,\% \pm 5\,\%$ from multiple experimental runs. Note that the helium concentration influences both the shock intensity and the amplitude growth and, therefore, affects the prediction of the freeze-out condition. In experiments, however, it is almost impossible to precisely control the helium concentration because helium has a much smaller molecular weight and diffuses much faster.

In the following studies, seven kinds of single-mode helium–air interface with different λ and a_0, as shown in table 1, are considered. For each case, according to the range of helium concentration in the undisturbed case, the freeze-out conditions of the single-mode helium–air interfaces with different initial conditions are predicted theoretically. Then multiple experimental runs are conducted until the experimental parameters satisfy the freeze-out condition. The parameters in each case in table 1 satisfy the small-perturbation hypothesis and the freeze-out condition. Specifically, the initial parameters in the former four cases (latter three cases) ensure the linear (weakly nonlinear) growth of the perturbation at the arrival of the reflected shock. Note that different initial conditions in weakly nonlinear cases from those in linear cases are selected, mainly because the perturbation with a larger wavelength needs more time to achieve freeze-out in weakly nonlinear cases. However, due to the limitation of the test section length, the time interval Δt cannot be regulated over a wide range in this work.

4.2. *The linear cases*

In this subsection, we consider the linear case, i.e. the perturbation growth of the shocked interface is in the linear stage at the arrival of the reflected shock. Specifically, four

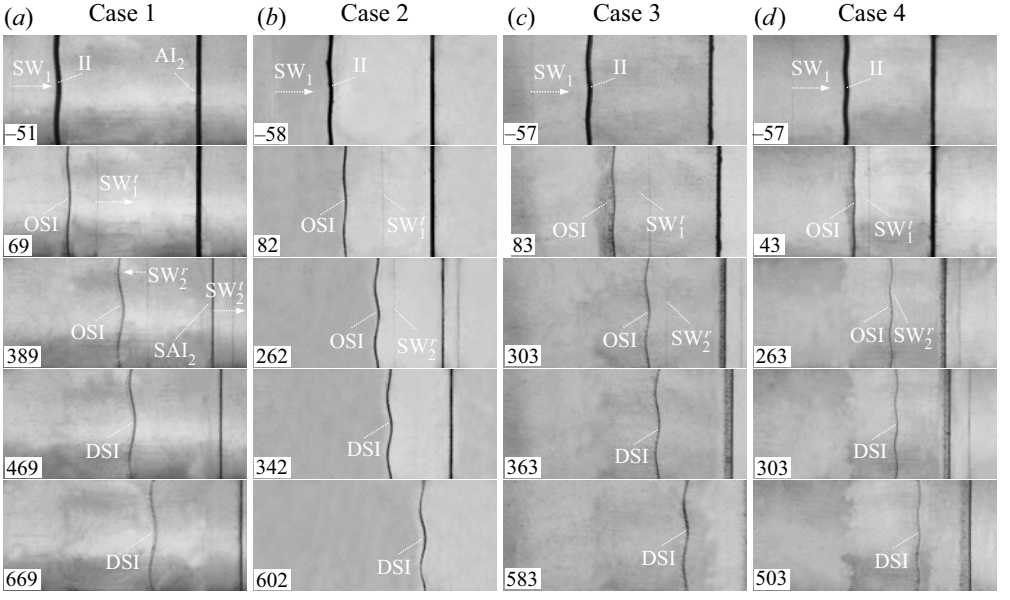

Figure 3. Typical schlieren images showing the interface evolution and wave patterns for cases 1–4. Here, SW_2^r is the shock of SW_1^t reflected from AI_2; SW_2^t is the shock of SW_1^t transmitted from AI_2; SAI_2 is the shocked AI_2; and DSI is the double-shocked interface. The contrast was enhanced without loss of trust.

single-mode helium–air interfaces with almost the same a_0/λ but different λ are studied (cases 1–4 in table 1). An air–SF_6 plane interface is adopted here to produce the reflected shock. The typical schlieren images of the helium–air interfaces accelerated by the incident shock and the reflected shock are provided in figure 3. Note that the shocked AI_1 is not shown in the images because it does not affect the perturbed interface evolution.

Taking case 1 as an example, when SW_1 interacts with II, a transmitted shock (SW_1^t) and a reflected shock are generated (69 μs). This reflected shock moving in helium is invisible due to its weak intensity. The shocked II (OSI) starts to move downstream with its amplitude increasing. Because the amplitude of II is small, SW_1^t quickly recovers to a planar shock. Subsequently, SW_1^t impacts AI_2, generating a transmitted shock (SW_2^t) and a reflected weak shock (SW_2^r) (389 μs). Before SW_2^r impact, the amplitude of the OSI grows continuously. After SW_2^r collides with the OSI, the amplitude almost stops growing (469–669 μs). In other words, the growth rate induced by SW_1 is eliminated completely by the reflected shock, and the amplitude growth is frozen out.

The variations of the dimensionless amplitudes in the different cases before and after the reflected shock impact are shown in figure 4(*a*). The time is normalized as $\tau = kv_i^e(t - t^*)$, where v_i^e is the linear growth rate of the OSI in experiments and t^* is the time when the linear growth of the OSI amplitude starts (generally compression phase ends). The amplitude is scaled as $\alpha = k(a - a^*)$, where a^* is the perturbation amplitude at $t = t^*$, which differs from the initial amplitude. From figure 4(*a*), the amplitudes of the OSI grow linearly before SW_2^r arrives. The linear growth rates of the OSI measured from the experiments and predicted from the impulsive model (Richtmyer 1960) are compared in table 2, and a good agreement is reached. After SW_2^r impacts the OSI, the amplitude rises again before it settles in the steady-state value in cases 1–3. Such a phenomenon, however, is absent in case 4. Note that the amplitude growth induced by the reflected shock needs a

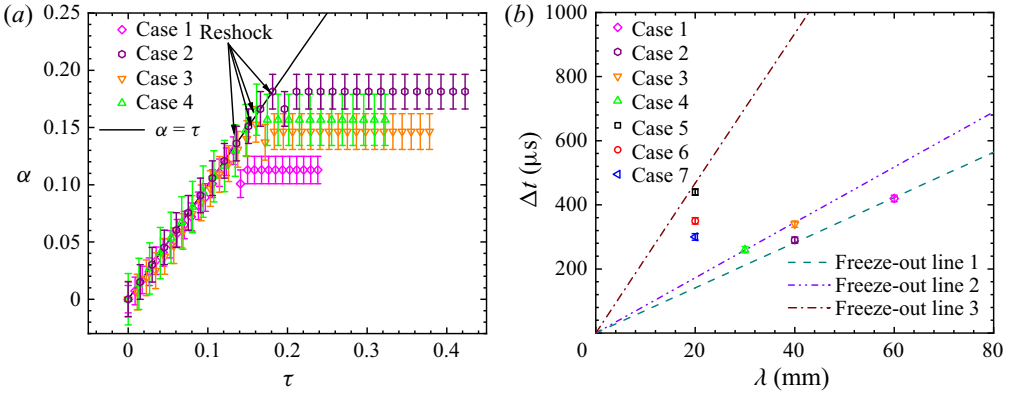

Figure 4. (*a*) Temporal variations of the dimensionless perturbation amplitude in cases 1–4. The solid line stands for the prediction from the impulsive model. (*b*) Freeze-out lines and distribution of initial parameters of different cases in the λ–Δt plane. Here, freeze-out lines 1, 2 and 3 correspond to cases 1 and 2, cases 3 and 4, and cases 5 to 7, respectively.

Case	1	2	3	4	5	6	7
v_i^e	4.21 ± 0.11	4.81 ± 0.10	3.65 ± 0.12	3.21 ± 0.20	3.36 ± 0.27	7.14 ± 0.66	10.59 ± 0.95
v_i^t	4.36	4.77	3.87	3.41	3.62	7.38	11.06

Table 2. Comparison of the linear growth rates of the OSI between experiments and predictions from the impulsive model.

start-up process (Lombardini & Pullin 2009). In cases 1–3, it is probable that the start-up process has not ended when the compression process ends, and the start-up process results in the rise of amplitude growth. In case 4, the wavelength is relatively smaller, and the start-up process is relatively shorter (Lombardini & Pullin 2009). The absence of the ascent process of amplitude growth is probably ascribed to the longer compression process than the start-up process. Besides, the limited temporal resolution in experiments may also cause this disparity. Although the amplitudes of these four cases are different, their growths are almost stagnated. As a result, freeze-out of amplitude growth of a single-mode helium–air interface is realized through a weak reflected shock in shock-tube experiments.

As indicated in § 2, if the perturbation growth is within the linear regime at the arrival of the reflected shock, λ and Δt satisfy a linear relationship. To verify this relation, the 'freeze-out lines' calculated by (2.6) are provided in figure 4(*b*). Note that the helium concentrations in cases 1 and 2 are different from those in cases 3 and 4; thus the freeze-out lines are therefore different, as indicated by freeze-out line 1 and freeze-out line 2, respectively. The experimental parameters are well located at the freeze-out lines, which experimentally verifies the linear relationship between λ and Δt. For each case, actually, more than two experimental runs are performed. We find that when freeze-out is achieved, the difference of Δt among cases is within 5 μs. According to this linear relationship, the initial parameters can be easily controlled to realize freeze-out.

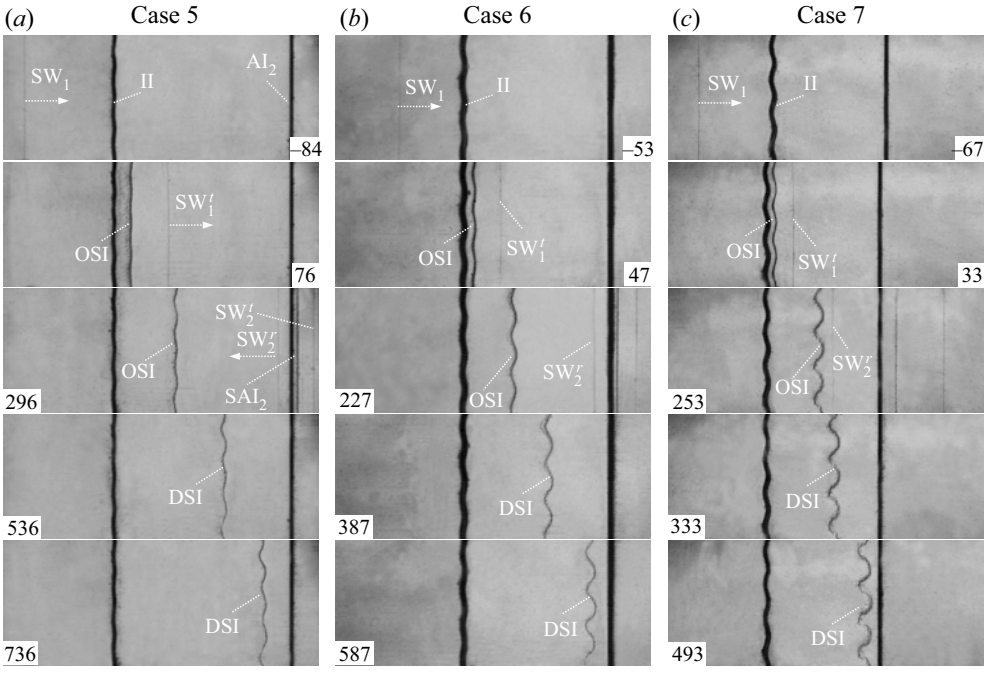

Figure 5. Typical schlieren images showing the interface evolution and wave patterns for cases 5–7.

4.3. *The weakly nonlinear cases*

In this subsection, the weakly nonlinear growth of the perturbation at the arrival of the reflected shock is considered. Three single-mode helium–air interfaces with the same small λ but different a_0 are tested (cases 5–7 in table 1). Because the growth rate in the weakly nonlinear regime is smaller than that in the linear regime, to offset the smaller growth rate, an even weaker reflected shock is needed. As a result, an air–argon interface, instead of an air–SF_6 interface, is adopted here to produce a weaker reflected shock. The weak reflected shock results in a longer Δt for the same L_0. A longer Δt and a smaller λ allow the amplitude to grow more quickly into the weakly nonlinear regime.

Figure 5 shows the evolutions of the single-mode helium–air interfaces accelerated by the incident shock and the reflected shock in cases 5–7. The wave patterns are quite similar to cases 1–4, and, therefore, the description is omitted. Taking case 7 as an example, before SW_2^r arrives (253 μs), the slightly asymmetric developments of the crest and trough occur, indicating the weakly nonlinear growth of the perturbation. After SW_2^r passes through the OSI (333 μs), the amplitude of the DSI remains almost constant. However, the interface profile changes with time, which is caused by the generation of the second-order harmonic (Liu *et al.* 2018). This will be discussed in the following paragraph.

Temporal variations of the dimensionless amplitude for cases 5–7 before and after SW_2^r impact are plotted in figure 6(*a*). Indeed, the perturbation growth enters the weakly nonlinear regime at the arrival of SW_2^r. The prediction from the ZG model is also included, and agrees well with the experimental results. As a result, the amplitude and growth rate of the OSI when the reflected shock arrives can be calculated by the ZG model (2.1*a*,*b*). After SW_2^r impinges upon the OSI, the ascent process of the amplitude growth is absent. In weakly nonlinear cases, the reflected shock is weaker and the amplitude is larger when the reflected shock arrives relative to linear cases. A relatively longer compression process

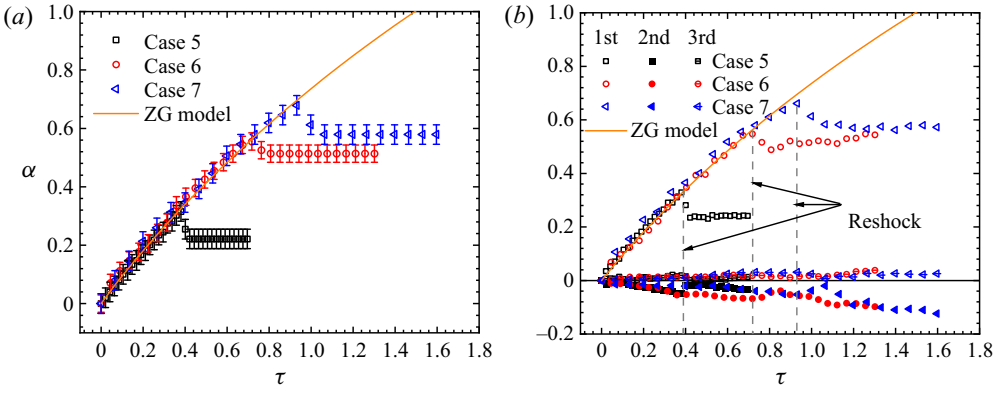

Figure 6. Temporal variations of the dimensionless amplitude before and after the reflected shock impact for the cases 5–7 (*a*) and amplitude developments for the first three harmonics (*b*).

may result in the absence of the ascent process, as explained in § 4.2. For cases 5–7, the amplitude growth almost stagnates, and freeze-out is realized. The Δt for achieving freeze-out predicted from the model for cases 5–7 are 435, 357 and 305 μs, respectively, which are in good agreement with the experimental counterparts, as given in table 1. This fact shows that, even if the perturbation growth is within the weakly nonlinear regime, freeze-out can still be achieved and predicted.

It is worth noting that when the OSI growth is weakly nonlinear, in order to realize freeze-out, Δt is related not only to λ but also to a_0. Therefore, a single freeze-out line does not exist. In figure 4, the freeze-out line 3 is calculated based on the initial parameters of $\varphi(\mathrm{He}) = 70\,\%$, $M_{s1} = 1.19$ and $M_{s2} = 1.02$. It is found that the Δt for cases 5–7 cannot be predicted by the linear relation (2.6), and, as the initial amplitude increases, the measured Δt deviates more from the freeze-out line. Figure 6(*b*) shows the amplitude growths of the first three harmonics. The amplitude of the fundamental mode is almost equal to the overall amplitude of the perturbation, and can be well predicted by the ZG model before the reflected shock impact. After the reflected shock impact, the amplitude growth of the fundamental mode nearly stagnates, but the amplitude of the second-order harmonic continues to grow, changing the interface profile. However, the second-order harmonic does not change the interface amplitude in the linear and weakly nonlinear stages (Guo *et al.* 2022), and thus will not affect the realization of freeze-out.

5. Conclusions

Freeze-out of amplitude growth of a shocked single-mode helium–air perturbation is realized through a weak reflected shock both theoretically and experimentally. Theoretically, two cases are considered. First, if the perturbation growth is within the linear regime when the reflected shock arrives (denoted as the linear cases), the impulsive model (Richtmyer 1960) and the linear model (Wouchuk & Nishihara 1997) are combined to calculate the relation among the initial parameters. It is found that the time interval Δt between the impacts of two shock waves is linearly related to the perturbation wavelength λ for achieving freeze-out, and is independent of the initial amplitude a_0. Second, if the perturbation growth is within the weakly nonlinear regime at the arrival of the reflected shock (denoted as the nonlinear cases), the nonlinear model (Zhang & Guo 2016) and the linear model (Wouchuk & Nishihara 1997) are adopted. It is found that Δt is related to both λ and a_0.

Experimentally, a light–heavy plane interface, instead of a rigid wall, is adopted to produce the weak reflected shock. The soap film technique is used to create the initially perturbed and undisturbed interfaces, and high-speed schlieren photography is used to capture the post-shock flow. Seven experimental runs, including four linear cases and three nonlinear cases, are considered. For the linear cases, the amplitude stops growing after the reflected shock impact, and the linear relationship between Δt and λ is verified experimentally. For the nonlinear cases, freeze-out can still be realized through a weaker reflected shock, but the linear relationship between Δt and λ does not exist. As a whole, a single-mode light–heavy perturbation can achieve amplitude freeze-out through a reflected shock. These findings may be helpful for better understanding how to suppress hydrodynamics instabilities in ICF. Note that only limited observations of this phenomenon are presented in the current work. More cases with a wider range of conditions will be tested in following work. Besides, the amplitude manipulation of a heavy–light interface subjected to a shock will also be investigated because in ICF the initial shock propagates from a heavy fluid to a light one.

Funding. This work was supported by the National Natural Science Foundation of China (nos. 12022201, 91952205 and 12102425) and Youth Innovation Promotion Association CAS.

Declaration of interests. The authors report no conflict of interest.

Author ORCIDs.
Zhigang Zhai https://orcid.org/0000-0002-0094-5210;
Xisheng Luo https://orcid.org/0000-0002-4303-8290.

References

Charakhch'yan, A.A. 2000 Richtmyer–Meshkov instability of an interface between two media due to passage of two successive shocks. *J. Appl. Mech. Tech. Phys.* **41**, 23–31.

Charakhch'yan, A.A. 2001 Reshocking at the non-linear stage of Richtmyer–Meshkov instability. *Plasma Phys. Control. Fusion* **43**, 1169–1179.

Guo, X., Cong, Z., Si, T. & Luo, X. 2022 Shock-tube studies of single- and quasi-single-mode perturbation growth in Richtmyer–Meshkov flows with reshock. *J. Fluid Mech.* **941**, A65.

Jacobs, J.W., Krivets, V.V., Tsiklashvili, V. & Likhachev, O.A. 2013 Experiments on the Richtmyer–Meshkov instability with an imposed, random initial perturbation. *Shock Waves* **23**, 407–413.

Leinov, E., Malamud, G., Elbaz, Y., Levin, L.A., Ben-Dor, G., Shvarts, D. & Sadot, O. 2009 Experimental and numerical investigation of the Richtmyer–Meshkov instability under re-shock conditions. *J. Fluid Mech.* **626**, 449–475.

Liang, Y. & Luo, X. 2021 On shock-induced light-fluid-layer evolution. *J. Fluid Mech.* **933**, A10.

Liang, Y., Zhai, Z., Ding, J. & Luo, X. 2019 Richtmyer–Meshkov instability on a quasi-single-mode interface. *J. Fluid Mech.* **872**, 729–751.

Lindl, J., Landen, O., Edwards, J., Moses, E. & NIC team 2014 Review of the national ignition campaign 2009–2012. *Phys. Plasmas* **21**, 020501.

Liu, L., Liang, Y., Ding, J., Liu, N. & Luo, X. 2018 An elaborate experiment on the single-mode Richtmyer–Meshkov instability. *J. Fluid Mech.* **853**, R2.

Lombardini, M. & Pullin, D.I. 2009 Startup process in the Richtmyer–Meshkov instability. *Phys. Fluids* **21**, 044104.

Meshkov, E.E. 1969 Instability of the interface of two gases accelerated by a shock wave. *Fluid Dyn.* **4**, 101–104.

Mikaelian, K.O. 1985 Richtmyer–Meshkov instabilities in stratified fluids. *Phys. Rev.* A **31**, 410–419.

Mikaelian, K.O. 2010 Analytic approach to nonlinear hydrodynamic instabilities driven by time-dependent accelerations. *Phys. Rev.* E **81**, 016325.

Mohaghar, M., Carter, J., Pathikonda, G. & Ranjan, D. 2019 The transition to turbulence in shock-driven mixing: effects of Mach number and initial conditions. *J. Fluid Mech.* **871**, 595–635.

Richtmyer, R.D. 1960 Taylor instability in shock acceleration of compressible fluids. *Commun. Pure Appl. Maths* **13**, 297–319.

WEBER, C., HAEHN, N., OAKLEY, J., ANDERSON, M. & BONAZZA, R. 2012 Richtmyer–Meshkov instability on a low Atwood number interface after reshock. *Shock Waves* **22**, 317–325.

WOUCHUK, J. & NISHIHARA, K. 1997 Asymptotic growth in the linear Richtmyer–Meshkov instability. *Phys. Plasmas* **4**, 1028–1038.

WOUCHUK, J.G. 2001 Growth rate of the Richtmyer–Meshkov instability when a rarefaction is reflected. *Phys. Plasmas* **8**, 2890–2907.

ZHANG, Q. & GUO, W. 2016 Universality of finger growth in two-dimensional Rayleigh–Taylor and Richtmyer–Meshkov instabilities with all density ratios. *J. Fluid Mech.* **786**, 47–61.

ZHOU, Y., *et al.* 2021 Rayleigh–Taylor and Richtmyer–Meshkov instabilities: a journey through scales. *Physica* D **423**, 132838.